JCTC Journal of Chemical Theory and Computation

Article

Cite This: J. Chem. Theory Comput. 2018, 14, 2947−2954

pubs.acs.org/JCTC

Efficient Automatized Density-Functional Tight-Binding Parametrizations: Application to Group IV Elements

Ahmad W. Huran,[†] Conrad Steigemann,[†] Thomas Frauenheim,[‡] Bálint Aradi,[‡] and Miguel A. L. Marques*[,†]

[†]Institut für Physik, Martin-Luther-Universität Halle-Wittenberg, D-06120 Halle (Saale), Germany

[‡]BCCMS, University of Bremen, 28359 Bremen, Germany

Supporting Information

ABSTRACT: Density-functional tight-binding methods stand out as a very good compromise between accuracy and computational efficiency. These methods rely on parameter sets that have to be determined and tabulated for every pair of chemical elements. We describe an efficient, and to a large extent automatic, procedure to build such parameter sets. This procedure includes the generation of unbiased training sets and subsequent optimization of the parameters using a pattern search method. As target for the optimization we ask that the formation energy and the forces on the atoms calculated within tight-binding reproduce the ones obtained using density-functional theory. We then use this approach to calculate parameter sets for group IV elements and their binaries. These turn out to yield substantially better results than previously available parameters, especially in what concerns energies and forces.

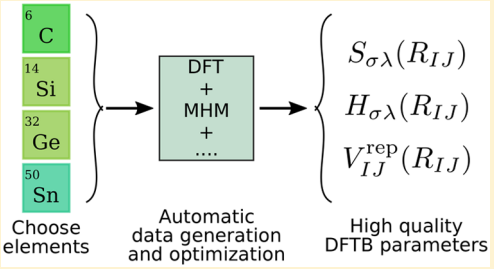

1. INTRODUCTION

The density-functional tight-binding method (DFTB)[1] along with its numerous extensions[2−15] constitutes an invaluable quantum-mechanical simulation tool kit. It mainly targets large molecular structures and extended systems with periodic boundary conditions involving up to tens of thousands of atoms in the unit cell.[16] Due to their ability to perform such large simulations while maintaining a quantum-mechanical description of the system, DFTB methodologies are valuable in a wide variety of research areas, from modeling chemical reactions[17−19] to biomolecular science,[20−22] solid-state physics,[23,24] and material science.[25−27]

At the core of all DFTB methodologies lies a very efficient approximation to density-functional theory (DFT).[28] This stems from expressing the wave functions as linear combinations of atomic orbitals from a tailored minimal basis-set (minimal-LCAO). Moreover, computation time is considerably reduced by precomputing and tabulating all the needed ingredients in the form of parameter sets known as Slater-Koster parameters.

Slater-Koster parameter sets need to be prepared beforehand for each pair of chemical elements to be considered. They contain an electronic part that is required for formulating the quantum-mechanical electronic-structure problem and a classical potential describing the repulsion between atomic cores and other terms of corrective nature. Conventionally, the parametrization of the electronic part is carried out explicitly only for the homonuclear case against some reference electronic-structure data,[29] while the heteronuclear parameters are built from the homonuclear ones.[24] While this kind of treatment reduces the work required for obtaining the electronic parameters, the repulsive potentials are still required for each pair of chemical elements. This turns out to be the most time-consuming step of the procedure. Multiple schemes were proposed[30−33] with the purpose of reducing human intervention in the parametrization procedure by automatizing, to different extents, the production of repulsive potentials.

One can also go a step further and fit the Slater-Koster parameters directly in order to reproduce some chosen properties of reference systems. Using this approach, ref 34 recently treated the parametrization procedure as a multi-objective optimization problem using a particle-swarm algorithm. This was found to yield very accurate parameters with respect to the relevant reference data.

Here we follow further this idea and propose a methodology to train DFTB parameters that are transferable (i.e., that can be used for a diversity of systems) and that yield accurate energies and forces. There are several steps in this methodology, starting with a careful preparation of unbiased training and test sets and subsequent optimization and testing of the parameters. Furthermore, a special emphasis was put into developing a robust and automated (black box) method, that can be easily applied to generate parameters for many pairs of elements. As an illustrative practical example we consider the parametrization of multiple DFTB models for the group IV elements (C, Si, Ge, Sn) and their binary combinations.

The rest of this Article is organized as follows. In section 2 we give a brief overview of the DFTB formalism, while the following section 3 is concerned with our strategy for the

Received: December 19, 2017
Published: May 7, 2018

DOI: 10.1021/acs.jctc.7b01269
J. Chem. Theory Comput. 2018, 14, 2947−2954

generation of the train and test sets and optimization of the DFTB parameters. We then present, in section 5, our results for group IV elements, both for elemental and binary phases. We complete the discussion with our conclusions.

2. DFTB

The original DFTB formulation[35,36] can be seen as a minimal LCAO two-center approximation to a zeroth-order perturbative expansion of the Kohn−Sham total energy[28] with respect to fluctuations around atomic charge densities. This treatment yields an energy E^{DFTB} that is given as the sum of a band-structure term E^{BS} and a pairwise repulsive potential E^{rep} (for a detailed derivation see refs 1 and 37)

$$E^{\mathrm{BS}} = \sum_i n_i \sum_{\sigma,\lambda} \overline{c}_{i\sigma} c_{i\lambda} \langle \varphi_\sigma | \hat{H}^{(0)}_{\mathrm{KS}} | \varphi_\lambda \rangle \tag{1a}$$

$$E^{\mathrm{rep}} = \frac{1}{2} \sum_{I,J}^{\mathrm{nuclei}} V^{\mathrm{rep}}_{IJ}(R_{IJ}) \tag{1b}$$

where the index i runs over Kohn−Sham orbitals with occupation numbers n_i, φ_σ and φ_λ are atomic orbitals used in the LCAO, and $\hat{H}^{(0)}_{\mathrm{KS}}$ is the Kohn−Sham Hamiltonian built from a superposition of either unperturbed reference densities or the corresponding potentials, with the two-center approximation being implicit. The term $V^{\mathrm{rep}}_{IJ}(R_{IJ})$ is a repulsive potential between atoms I, J, and R_{IJ} is the respective internuclear distance. The perturbative expansion mentioned above can be truncated at second order, including to lowest order the contribution of charge-density fluctuations to the total energy.

Effects related to charge-transfer can be handled by the self-consistent-charge (SCC) extension to DFTB.[2] The SCC DFTB energy is given by

$$E^{\mathrm{DFTB}}_{\mathrm{SCC}} = E^{\mathrm{DFTB}} + \frac{1}{2} \sum_{I,J}^{\mathrm{nuclei}} \gamma_{IJ}(R_{IJ}) \Delta q_I \Delta q_J \tag{2}$$

where $\gamma_{IJ}(R_{IJ})$ represents the effective interaction between two spherical charge distributions at the distance R_{IJ}.[32] This is computed from the Hubbard parameters of the free, spin-unpolarized atoms I and J.[2] Finally Δq_I is the Mulliken charge of atom I.

Atomic charge densities and atomic orbitals are conventionally obtained from the solution of the Kohn−Sham equations for the atom in a confinement potential using Slater-type orbital basis.[38] Typically, the confinement potential is a spherical power potential of the form

$$V_{\mathrm{power}}(r) = \left(\frac{r}{r_0}\right)^n \tag{3}$$

The confinement power n and the confinement radius r_0 are parameters of the DFTB model and can be chosen, e.g., to reproduce DFT band structures.[29] It was found that rather steep confinement potentials were needed.

Another confinement potential that is gaining popularity is the Woods-Saxon potential[39]

$$V_{\mathrm{WS}}(r) = \frac{h}{1 + \mathrm{e}^{-a(r-r_0)}} \tag{4}$$

where h is the asymptote of the potential as $r \to \infty$, r_0 is the inflection radius, and a is proportional to the slope at the inflection radius. First introduced in the context of relativistic SCC DFTB as a possible alternative to the incompatible power potentials,[40] it was later shown to reproduce accurately band structures of various materials at different levels of theory.[34]

Having obtained a satisfactory parametrization of the band-structure contribution to the energy, one is left with the pairwise repulsive potentials. Usually, these potentials are prepared manually and represented by cubic splines (for a detailed procedure see ref 41). In this work we will follow the approach of Bodrog et al.[32] and express each pairwise repulsive potential as a linear combination of cutoff polynomials

$$V^{\mathrm{rep}}_{IJ}(\phi^{\mathrm{rep}}_{IJ}, R_{IJ}) = \sum_{\nu=2 \text{ or } 3} \phi^{\mathrm{rep}}_{\mathrm{IJ},\nu}(R^{\mathrm{cut}}_{IJ} - R_{IJ})^\nu \tag{5}$$

where R^{cut}_{IJ} is the cutoff of the potential V^{rep}_{IJ}, and ϕ^{rep}_{IJ} is a set of coefficients to be determined. It has been shown that this approach yields repulsive potentials comparable to the handmade ones if not better.[32] Furthermore, this particular choice allows for a very fast construction of repulsive potentials.

To add flexibility to the optimization of the electronic terms, we can also fit directly the Slater-Koster parameters. This approach is close in spirit to the conventional tight-binding way of building the Hamiltonian and overlap matrices. Here we consider only the nonzero off-diagonal elements to be free parameters, while maintaining the diagonal of the Hamiltonian. In this manner the DFT limit is approached as the internuclear separation grows larger. To model the distance-dependent matrix elements we propose the form

$$M(R_{IJ}) = \mathrm{e}^{-\alpha R_{IJ}} \sum_{\nu=0} c_\nu (R_0 - R_{IJ})^\nu \tag{6}$$

where $M(R_{IJ})$ is a matrix element between two basis functions centered on atoms I and J, R_{IJ} is the distance between the atomic centers, and α, R_0, and c_ν are free parameters.

The form given by eq 6 was chosen to reduce to existing DFTB electronic parametrizations while using a moderate number of free parameters. A typical number of terms is 10−13 for a total of 12−15 free parameters per matrix element. The number of parameters is rather large especially for the heteronuclear case. Nevertheless, if one uses as the starting point a reasonable guess for the Hamiltonian and overlap matrix elements (for example, from an existing DFTB parametrization), the optimization can be performed efficiently. We will call the parameter sets obtained in this way "fully unconstrained", while the ones obtained with a confining potential will be referred to as "standard".

3. TRAIN AND TEST SETS

In this section we discuss how we generate our training sets (used to fit the tight-binding parameters) and our testing sets (used to assess the quality of the fitted parameters). Note that it is very important to use two completely different sets in order to check for any problem related to overfitting of the data. Our main interest is to obtain good energies and forces, as these are the quantities that are relevant for molecular dynamics or global structural prediction. Therefore, our data sets are designed to include a wide, and unbiased, range of crystal structures that are characteristic of the different atomic arrangements that can appear in such simulations. The training data is obtained at the level of DFT with the Perdew−Burke−Ernzerhof[42] approximation to the exchange-correlation functional as implemented in the VASP code.[43] We used the PAW pseudopotentials of

DOI: 10.1021/acs.jctc.7b01269
J. Chem. Theory Comput. 2018, 14, 2947−2954

version 5.2 of VASP and dense *k*-point sets that yield a precision of around 2 meV/atom in the total energy.

Generation of the reference data sets was carried out in two separate steps. The first step of the process uses a global structural prediction method[44] to explore the possible bonding patterns and crystal structures allowed by the chemical composition. Specifically, we use the minima-hopping method (MHM),[45,46] an efficient approach that has been frequently used in the past years to discover new materials and crystal phases.[16,26,47] We recall that this method uses a walker in configuration space and that it proceeds by a series of short molecular dynamics (MD) simulations followed by geometry optimization steps. The output of our runs includes therefore not only a set of structures corresponding to local-minima (loc-min) but another set of intermediate structures resulting from molecular dynamics runs. Note that the majority of structures is far from dynamical equilibrium.

For efficiency reasons we used a rather small number of atoms in the unit cell for the simulations, and we stopped our minima hopping runs relatively early (after ∼30−80 minima were found). We note, however, that our objective is merely to sample possible crystal structures and not to do extensive explorations of the phase diagram; therefore, such relatively inexpensive simulations are more than sufficient. For elementary substances, we performed one run with 1 and 2 atoms in the unit cell and two runs with 4, 5, and 6. To add to the structural variety, we also performed two runs at the pressure of 20 GPa, one with 4 and another with 6 atoms in the unit cell. For binary systems composed of elements A and B, we ran calculations for all compositions that yield at most 6 atoms in the unit cell. This amounted to the following stoichiometries: AB (2 and 3 formula units per unit cell), A_2B and AB_2 (2 formula units per unit cell), and A_3B, AB_3, A_4B, AB_4, A_5B, AB_5, A_2B_3, and A_3B_2 (1 formula unit per unit cell). Two minima hopping runs were performed for each of these cases.

To complement our data sets, and in the spirit of ref 48, we then apply a series of geometrical distortions to the local minima. Finally, we add to the loc-min subset of the elementary substances a set of two-dimensional minima structures obtained with the procedure of ref 26. In this way, we expect to increase the transferability of our parameters to structures with lower coordination.

From this wealth of data we then select randomly two nonoverlapping sets with the same size (one for fitting and another of the same size for testing). Our only requirement is that the maximum force acting on the atoms is less or equal than 2 eV/Å (as these highly unstable structures are unlikely to be important in any simulation). The set that contains the shortest internuclear distance is used as a fitting set, as the repulsive potential bears little meaning at distances much shorter than the shortest distance present in the fitting set. Detailed specifications about the train (and test) sets are listed in Table 1 for all systems studied here.

Table 1. Number and Type of Structures Included in the Train and Test Data Sets for the Considered Species[a]

	loc-min	distorted	MD	total
C	62	200	200	462
Si	84	200	200	484
Ge	89	200	200	489
Sn	82	200	200	482
AB	100	200	200	500

[a]AB refers to any of the binary phases considered.

4. AUTOMATIZED PARAMETRIZATION

The fact that a repulsive potential (or the matrix elements of eq 6) needs to be built for each pair of atom-types dictates that the number of potentials grows quadratically with the number of elements to be considered. Hence, making large parameter sets or systematically extending existing ones becomes intractable rather quickly. Automatized parametrization aims at reducing human intervention in the process to facilitate producing and maintaining large parameter sets.

Having in mind applications in the field of molecular dynamics or global structural prediction, we consider two objectives in the optimizations. The first is the square of the weighted average L^2 norm of the error committed by DFTB in computing formation energies ΔE per atom, with respect to the DFT ones

$$\mu_{\Delta E} = \frac{\sum_i w_i (\Delta E_i^{\mathrm{DFT}} - \Delta E_i^{\mathrm{DFTB}})^2}{\sum_i w_i} \tag{7}$$

where the sum over i runs over all structures under consideration each with a weight w_i. The second objective is the analogue concerning the forces

$$\mu_F = \frac{\sum_i \sum_j^{N_i} \frac{w_i}{3N_i} \sum_q^3 (F_{ijq}^{\mathrm{DFT}} - F_{ijq}^{\mathrm{DFTB}})^2}{\sum_i w_i} \tag{8}$$

where the index q denotes a Cartesian component of the force vector $\mathbf{F}_{ij}$ acting on the j^{th} atom in the i^{th} structure that has N_i total number of atoms.

Both objectives were visible to the optimization procedure as a linearly scalarized single objective using equal weights

$$\mu = \mu_{\Delta E} + \mu_F \tag{9}$$

It should be mentioned that linear-scalarization of multi-objectives can yield Pareto-optimal solutions only on the convex regions of the corresponding Pareto front.[49,50] However, we found that linearly scalarizing the formation energy and force objectives with equal weights yields satisfying results.

We expect that regions of phase-space close to the dynamical minima are sampled most often in simulations. Therefore, to obtain a better description of these regions we decided to include in our objectives a dimensionless weight factor w_i that is given in terms of $\overline{F}_i$ the average norm of forces acting on atoms in the i^{th} structure. It reads, when $\overline{F}_i$ is measured in eV/Å

$$w_i = \frac{0.2}{0.2 + \overline{F}_i^2} \tag{10}$$

This function attains its maximum value of one for $\overline{F}_i = 0$ and decreases monotonically for larger forces.

Searching for an appropriate method to solve our optimization problem, we experimented with genetic algorithms,[51] particle-swarm optimization,[34] and surrogate-model based algorithms,[52,53] among others. We found that a pattern-search algorithm,[54] using a coordinate-basis for the pattern, is very suitable in terms of the quality of the solution and the time needed to reach it. Although pattern-search methods are typically considered to be local-optimization methods, they can show global-identification behavior[55] to some extent. A detailed description of pattern-search algorithms can be found in ref 56 and ref 57.

DOI: 10.1021/acs.jctc.7b01269
J. Chem. Theory Comput. 2018, 14, 2947−2954

5. RESULTS AND DISCUSSION

All DFTB calculations were carried out using the DFTB+ code.[58] For the calculations we used a dense k-point mesh of 4 k-points/Å^{-1} as generated by the atomic simulation environment.[59] A tolerance of 10^{-5} for the SCC cycle was used with 30 iterations at most, with a Broyden mixing parameter of 0.4.

The optimization of the electronic part of the DFTB model was carried out using the SCOLIB implementation of the pattern-search algorithm, employing a coordinate-basis for its pattern, via the DAKOTA tool kit.[55]

5.1. Elemental Phases. We start our discussion with the parametrizations of the elemental phases of the group IV elements (C, Si, Ge, and Sn). To obtain the electronic part of the DFTB model we chose a shell-resolved Woods-Saxon confinement potential, with an extra confinement potential of the same type for calculating charge densities. The powers of polynomial terms in the repulsive potentials were kept constant during the optimization, namely we used a ninth degree polynomial with minimal power of 3. Cutoff values of the repulsive potentials were fixed at 4.0, 5.0, 5.5, and 6.0 au for C−C, Si−Si, Ge−Ge, and Sn−Sn, respectively. Those values were loosely chosen according to the usual convention to go slightly beyond first neighbors. The optimization was carried out using non-SCC DFTB. As an initial guess for the confinement potentials we have used a value of 1 au for all the parameters. The resulting parameters of the confinement potentials for the elemental phases are reported in Table 2.

Table 2. Resulting Parameters of the Confinement Potentials[a]

element		a	r_0	W
C	density	1.0604	0.5942	0.9990
	s	3.9339	0.7321	3.2960
	p	1.9646	2.8762	1.9716
Si	density	1.0000	1.0000	1.0000
	s	5.0781	3.5828	2.7219
	p	1.7703	1.0000	1.9516
	d	1.1359	1.0000	4.4437
Ge	density	1.7023	1.0000	1.0000
	s	2.9824	3.4695	1.1133
	p	1.8723	1.0000	2.5519
	d	1.3625	1.0000	5.7125
Sn	density	1.0000	1.0113	1.0000
	s	1.0000	1.8043	1.0113
	p	1.0113	1.0000	2.6369
	d	1.2945	1.0000	6.3469

[a]All values are in au.

Having obtained a satisfactory parametrization of the confinement potentials, we perform the (computationally inexpensive) optimization of the repulsive potentials. We perform several runs varying the number of polynomial terms in the repulsive potentials. The best parametrization is then chosen, ensuring that it does not have spurious oscillations, and that it has positive curvature at short internuclear distances.

The parametrization of the fully unconstrained parameter sets was performed in a similar fashion, using 18, 10, 13, and 18 terms in the electronic part for C, Si, Ge, and Sn, respectively.

The parameter sets are then benchmarked. From Table 3 we can see that the average errors in the train and test sets are comparable, indicating that there is no overfitting. This is true also for the fully unconstrained optimizations that use a substantially larger amount of parameters. Errors in the energy are between ∼20−60 meV/atom, with carbon exhibiting an error twice as large as the other three group IV elements. This can be attributed to the richer chemistry of carbon, leading to the known poorer transferability of the parameters.[29] Note that these are rather small errors, considerably smaller than the average error in PBE formation energies.[60−62] A similar trend can be obtained by looking at the errors in the forces. These range from around 40 to 160 meV/Å, again with C, that forms the strongest bonds of group IV, at the top of this range.

Table 3. Errors in the Formation Energy (meV/atom) and Forces (meV/Å) for the Considered Elemental Phases Evaluated for the Training and the Testing Data Sets[a]

		$\sqrt{\mu_{\Delta E}}$		$\sqrt{\mu_F}$	
	type	train	test	train	test
C	standard	52.4	62.7	161.7	138.4
	fully unconstr	42.1	39.1	130.4	117.5
Si	standard	32.8	37.8	71.2	71.5
	fully unconstr	23.9	28.7	59.3	60.9
Ge	standard	27.3	24.9	56.6	54.1
	fully unconstr	17.8	16.2	42.8	41.6
Sn	standard	33.7	34.9	42.9	45.9
	fully unconstr	26.5	28.1	41.7	45.0

[a]For each element we present results for the standard and for the fully unconstrained parametrizations.

We now compare our results against some popular SCC DFTB parametrizations such as pbc-0-3,[63,64] matsci-0-3,[65] and the third-order[9] 3ob-3-1[66] (that will be used here without including third-order corrections). For consistency, we prepared SCC consistent repulsives for our electronic parametrization described above. The difference to the non-SCC parametrizations is, as expected, minor, as can be seen by comparing Tables 3 and 4.

Table 4. Comparison of the Errors in Formation Energies (meV/atom) and the Forces (meV/Å) at the SCC DFTB Level for the Considered Elemental Phase[a]

	type	$\sqrt{\mu_{\Delta E}}$	$\sqrt{\mu_F}$
C	this work	61.1	134.4
	pbc-0-3	419.2	257.4
	matsci-0-3	466.7	275.7
	3ob-3-1	122.2	206.2
Si	this work	37.5	70.9
	pbc-0-3	384.3	240.4
	matsci-0-3	1137.1	766.2
Ge	this work	25.2	53.7
Sn	this work	35.5	45.4

[a]These values were evaluated for the testing data sets using both our "standard" parameters and other parameters found in the literature.

Our parameter sets perform consistently better than all previous parametrizations. For carbon, the 3ob-3-1 set is the closest to our results. The pbc-0-3 and matsci-0-3 sets are comparable to each other, with the matsci-0-3 ones being slightly worse. This was expected, as the pbc-0-3 set was prepared with extended systems in mind. For silicon, the pbc-0-3 set yields comparable results to carbon, while the matsci-0-3 is clearly inadequate for describing solid silicon phases.

DOI: 10.1021/acs.jctc.7b01269
J. Chem. Theory Comput. 2018, 14, 2947−2954

Although we did not consider the band structure as one of the objectives of our optimization, it is interesting to see how our parameters perform for this property. It turns out that they reproduce fairly well the band structures of typical representatives of the considered phases. In Figure 1 we

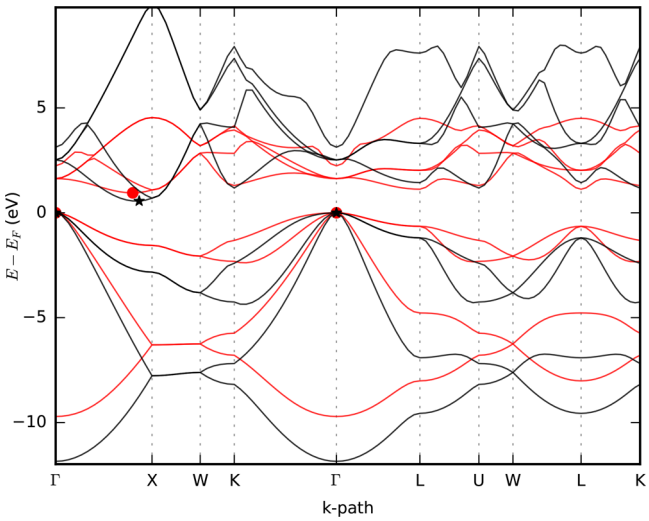

Figure 1. Band structure of diamond Si computed using DFT within the PBE approximation (in black) and our "standard" DFTB parameters (in red). The indirect gap is shown by star and circle markers for DFT and DFTB, respectively.

show a comparison for the band structure of silicon in the cubic diamond phase, calculated with both DFT and DFTB with our parameters. The DFTB valence bands are similar to the DFT ones, the main difference being a compression of the band widths. The DFTB conduction bands have their minimum close to the DFT results, yielding correctly Si as an indirect semiconductor. The DFTB band gap is also in good agreement with the DFT one. The fact that the pbc-0-3 set yields a direct band gap for silicon can be attributed to the lack of a full treatment of *d* orbitals. However, pbc-0-3 was shown to yield HOMO−LUMO gaps that supersedes in quality gaps from semiempirical methods[67] such as PM6[68] for silicon nanocrystals.

Other band structures for C, Si, Ge, and Sn in the diamond cubic structure can be found in the Supporting Information. It turns out that the "standard" parametrizations outperform the "fully unconstrained" ones. This was to be expected, as the latter are optimized much more aggressively to reproduce formation energies and forces. In any case, we do not recommend the use of these parametrizations for the investigation of the electronic structure. A much better approach would be, of course, to develop Slater-Koster parameters by including the band structure as a target for the optimization.

5.2. Binary Phases. Two sets of repulsive parameters were prepared using our "standard" and "fully unconstrained" recipes.

In standard DFTB, the Slater-Koster parameters for a heteronuclear pair are, as for the homonuclear case, calculated directly from the orbitals of the individual constrained atoms. In view of the variety of possible binding patterns, we can expect a deterioration of the quality of parameters and a reduction of the transferability for binary phases. This is what we can observe in Table 5, where we present the errors using the test set for our

Table 5. Error in the Formation Energy (meV/atom) and Force (meV/Å) for the Considered Binary Combinations Evaluated in the Testing Data Sets[a]

	type	$\sqrt{\mu_{\Delta E}}$	$\sqrt{\mu_F}$
C−Si	standard	132.5	284.5
	fully unconstr	37.8	197.3
	pbc-0-3	176.4	400.1
C−Ge	standard	258.2	250.3
	fully unconstr	34.8	165.1
C−Sn	standard	356.2	289.6
	fully unconstr	45.5	184.8
Si−Ge	standard	32.6	74.7
	fully unconstr	18.2	56.2
Si−Sn	standard	52.4	115.2
	fully unconstr	25.4	80.0
Ge−Sn	standard	26.6	69.5
	fully unconstr	17.3	63.0

[a]Results for the pbc-0-3 set are also given for C−Si.

"standard" parametrizations. In this case, we used as cutoffs for the repulsive potentials, 4.5, 4.5, 5.0, 5.0, 5.0, and 5.5 au for C−Si, C−Ge, C−Sn, Si−Ge, Si−Sn, and Ge−Sn, respectively. Although our "standard" parameters still work considerably better than the pbc-0-3, there is a remarkable increase in the errors for both energies and forces, when comparing with the results for elemental substances of Table 3. The most drastic deterioration of quality is apparent in species containing carbon.

One possible source of error is the use of a non-SCC treatment. We investigated this problem by creating SCC parametrizations and calculating the corresponding errors for the test sets. It is true that the error decreases but unfortunately by a relatively small amount. A more successful approach consisted in treating the electronic parameters as independent variables, independent of the homonuclear parametrization. This is possible via the fully unconstrained procedure explained before. In this case, the optimization of the electronic parameters was carried out using 10 terms for each matrix element in the case of C−Si, C−Ge, Si−Ge, Si−Sn, and Ge−Sn, while 13 terms were employed for C−Sn. In this way the error in both energies and forces decreases considerably to values similar to the homonuclear case above.

5.3. Further Tests. To further verify the transferability of the generated parameter sets we assess their quality using data sets of group IV ternary compounds. The data sets were randomly selected from structural prediction runs, with a maximum average force of ∼1 eV. The data sets consist of 171, 128, 128, 115 of C−Si−Ge, C−Si−Sn, C−Ge−Sn, and Si−Ge−Sn structures, respectively. Results are collected in Table 6. We observe a trend similar to the binary compounds, with carbon containing species exhibiting the errors of largest magnitude. As one would expect, the error increases when considering ternary compounds. However, it is still perfectly within reasonable limits (especially for the fully unconstrained parametrizations), indicating good transferability of the parameters.

Using the Murnaghan equation of state,[69] we calculated bulk moduli and equilibrium cell volumes for some selected systems in the cubic diamond lattice. The Brillouin-zone sampling was carried out using a 10 × 10 × 10 Monkhorst−Pack grid. In Table 7 we collect the errors (in %) for the bulk modulus and the volume of the primitive unit cell, compared to the

DOI: 10.1021/acs.jctc.7b01269
J. Chem. Theory Comput. 2018, 14, 2947−2954

Table 6. Error in the Formation Energy (meV/atom) and Force (meV/Å) for the Considered Ternary Combinations at the Non-SCC Level

	type	$\sqrt{\mu_{\Delta E}}$	$\sqrt{\mu_F}$
C−Si−Ge	standard	204.2	297.7
	fully unconstr	50.7	191.1
C−Si−Sn	standard	244.8	416.2
	fully unconstr	80.2	265.0
C−Ge−Sn	standard	367.5	347.3
	fully unconstr	90.0	241.4
Si−Ge−Sn	standard	66.1	122.9
	fully unconstr	15.8	91.6

Table 7. Errors in the Bulk Modulus and the Volume of the Primitive Unit Cell Volume in the Cubic Diamond Lattice

	$\Delta B/B_{\mathrm{PBE}}$ (%)		$\Delta V_0/V_0^{\mathrm{PBE}}$ (%)	
	standard	fully unconstr	standard	fully unconstr
C	5.54	−1.39	−0.18	0.35
Si	−8.01	−5.82	−2.64	−2.23
Ge	−12.96	−4.45	0.02	−2.44
Sn	−15.27	13.41	3.48	−1.53

corresponding DFT results (for the raw data see the Supporting Information). The errors in the lattice constant are in general rather small for both sets of parameters and are never larger than a few percent. Errors for the bulk modulus are considerably larger, as this quantity is more sensitive to small variations. They are between 1−15% and are slightly better for the fully unconstrained parameters.

Phonon dispersion curves were calculated for the same systems by the finite differences method via the phonopy package[70] using 4 × 4 × 4 supercells. All results can be found in the Supporting Information. The DFT phonon dispersion curves are in general quite well described, with the fully unconstrained parameters yielding errors for the highest optical frequencies that are usually below 10%.

Finally, we take a look at the Slater-Koster parameters themselves (see the Supporting Information for a complete set of plots of the Slater-Koster parameters). It is well-known that a direct optimization can lead to unphysical features. This includes spurious oscillations, deviations of large magnitude, or even a change of sign, when compared to integrals computed from physical wave functions. We try to avoid these problems by carrying out our fully unconstrained optimizations within tight bounds in the parameter space around the initial guess. This recipe, however, is not foolproof due to the nonlinear nature of the problem. In most of the obtained Slater-Koster parameters, this procedure proved successful. However, in a few situations, artifacts, and in particular a change of sign of the curves, were observed. This again indicates that it is not advisible to use our fully unconstrained parameters to calculate other properties than the ones they were fitted to, namely total energies and forces (and derived quantities).

6. CONCLUSION

We present an efficient, and highly automatized, approach to obtain optimized parametrizations to be used in the density-functional tight-binding method. There are several steps in this approach: (i) Train and test sets are built using density-functional theory. To ensure that these sets include structures representative of all bonding possibilities, these are generated from short global structural prediction runs. (ii) An algorithm based on the pattern-search method is then used to optimize the parameters. (iii) These parameters are then tested for the structures contained in the test set to avoid problems of overfitting.

A model functional form for matrix elements was also proposed that grants extra variational freedom in the density-functional tight-binding model allowing for the fine-tuning of the electronic parameters. It was shown that this fully unconstrained optimization brings significant improvements especially for binary and ternary systems.

The resulting procedure was applied to the group IV elements (C, Si, Ge, and Sn), and their binary combinations. As optimization targets we used formation energies and forces acting on the atoms. The resulting parameters show remarkable improvements, both in formation energies and forces, over some of the popular parametrizations present in the literature. Finally, to assess transferability of the obtained parameter sets, they were tested against bulk moduli and unit cell volumes for some selected systems and against formation energies and forces of group IV ternary compounds. We believe that the quality of the produced parameter sets makes them particularly suitable for their use in molecular dynamics and structural studies.

■ ASSOCIATED CONTENT

Supporting Information

The Supporting Information is available free of charge on the ACS Publications website at DOI: 10.1021/acs.jctc.7b01269.

More band-structure examples, phonon dispersion curves, and raw data used in Table 7 (PDF)

Complete set of figures comparing the fully unconstrained Slater-Koster parameter set against the standard one (PDF)

Archive containing all the structures used in this work in `.cif` format (ZIP)

■ AUTHOR INFORMATION

Corresponding Author

*E-mail: miguel.marques@physik.uni-halle.de.

ORCID

Miguel A. L. Marques: 0000-0003-0170-8222

Funding

M.A.L.M. and A.W.H. acknowledge partial support from the German Research Foundation within the Collaborative Research Centre 762 (project A11).

Notes

The authors declare no competing financial interest.

■ REFERENCES

(1) Foulkes, W. M. C.; Haydock, R. Tight-binding models and density-functional theory. *Phys. Rev. B: Condens. Matter Mater. Phys.* **1989**, *39*, 12520−12536.

(2) Elstner, M.; Porezag, D.; Jungnickel, G.; Elsner, J.; Haugk, M.; Frauenheim, T.; Suhai, S.; Seifert, G. Self-consistent-charge density-functional tight-binding method for simulations of complex materials properties. *Phys. Rev. B: Condens. Matter Mater. Phys.* **1998**, *58*, 7260−7268.

(3) Köhler, C.; Seifert, G.; Frauenheim, T. Density functional based calculations for Fe_n ($n \leq 32$). *Chem. Phys.* **2005**, *309*, 23−31.

(4) Köhler, C.; Frauenheim, T.; Hourahine, B.; Seifert, G.; Sternberg, M. Treatment of collinear and noncollinear electron spin within an

DOI: 10.1021/acs.jctc.7b01269
J. Chem. Theory Comput. 2018, 14, 2947−2954

approximate density functional based method. *J. Phys. Chem. A* **2007**, *111*, 5622−5629.
(5) Cui, Q.; Elstner, M.; Kaxiras, E.; Frauenheim, T.; Karplus, M. A QM/MM Implementation of the Self-Consistent Charge Density Functional Tight Binding (SCC-DFTB) Method. *J. Phys. Chem. B* **2001**, *105*, 569−585.
(6) Han, W.-G.; Elstner, M.; Jalkanen, K. J.; Frauenheim, T.; Suhai, S. Hybrid SCC-DFTB/molecular mechanical studies of H-bonded systems and of N-acetyl-(L-Ala)nN'-methylamide helices in water solution. *Int. J. Quantum Chem.* **2000**, *78*, 459−479.
(7) Elstner, M.; Hobza, P.; Frauenheim, T.; Suhai, S.; Kaxiras, E. Hydrogen bonding and stacking interactions of nucleic acid base pairs: a density-functional-theory based treatment. *J. Chem. Phys.* **2001**, *114*, 5149−5155.
(8) Hourahine, B.; Sanna, S.; Aradi, B.; Köhler, C.; Niehaus, T.; Frauenheim, T. Self-interaction and strong correlation in DFTB. *J. Phys. Chem. A* **2007**, *111*, 5671−5677.
(9) Yang, Y.; Yu, H.; York, D.; Cui, Q.; Elstner, M. Extension of the self-consistent-charge density-functional tight-binding method: Third-order expansion of the density functional theory total energy and introduction of a modified effective coulomb interaction. *J. Phys. Chem. A* **2007**, *111*, 10861−10873.
(10) Niehaus, T. A.; Suhai, S.; Della Sala, F.; Lugli, P.; Elstner, M.; Seifert, G.; Frauenheim, T. Tight-binding approach to time-dependent density-functional response theory. *Phys. Rev. B: Condens. Matter Mater. Phys.* **2001**, *63*, 085108.
(11) Trani, F.; Scalmani, G.; Zheng, G.; Carnimeo, I.; Frisch, M. J.; Barone, V. Time-dependent density functional tight binding: new formulation and benchmark of excited states. *J. Chem. Theory Comput.* **2011**, *7*, 3304−3313.
(12) Nishizawa, H.; Nishimura, Y.; Kobayashi, M.; Irle, S.; Nakai, H. Three pillars for achieving quantum mechanical molecular dynamics simulations of huge systems: Divide-and-conquer, density-functional tight-binding, and massively parallel computation. *J. Comput. Chem.* **2016**, *37*, 1983−1992.
(13) Wu, Y.; Ilie, A.; Crampin, S. Self-consistent charge and dipole density functional tight binding method and application to carbon-based systems. *Comput. Mater. Sci.* **2017**, *134*, 206−213.
(14) Lutsker, V.; Aradi, B.; Niehaus, T. A. Implementation and benchmark of a long-range corrected functional in the density functional based tight-binding method. *J. Chem. Phys.* **2015**, *143*, 184107.
(15) Kranz, J. J.; Elstner, M.; Aradi, B.; Frauenheim, T.; Lutsker, V.; Garcia, A. D.; Niehaus, T. A. Time-Dependent Extension of the Long-Range Corrected Density Functional Based Tight-Binding Method. *J. Chem. Theory Comput.* **2017**, *13*, 1737−1747.
(16) Sakti, A. W.; Nishimura, Y.; Nakai, H. Divide-and-conquer-type density-functional tight-binding simulations of hydroxide ion diffusion in bulk water. *J. Phys. Chem. B* **2017**, *121*, 1362−1371.
(17) Sakti, A. W.; Nishimura, Y.; Sato, H.; Nakai, H. Divide-and-Conquer Density-Functional Tight-Binding Molecular Dynamics Study on the Formation of Carbamate Ions during CO2 Chemical Absorption in Aqueous Amine Solution. *Bull. Chem. Soc. Jpn.* **2017**, *90*, 1230−1235.
(18) Marutaphan, A.; Seekaew, Y.; Wongchoosuk, C. Self-Consistent Charge Density Functional Tight-Binding Study of Poly (3, 4-ethylenedioxythiophene): Poly (styrenesulfonate) Ammonia Gas Sensor. *Nanoscale Res. Lett.* **2017**, *12*, 90.
(19) Li, J.; Foster, M. E.; Sohlberg, K. Density-functional based tight-binding for the study of CO2/MOF interactions: the case of Zn (ADC)· DMSO. *Mol. Simul.* **2017**, *43*, 428−438.
(20) Gaus, M.; Cui, Q.; Elstner, M. Density functional tight binding: application to organic and biological molecules. *Wiley Interdiscip. Rev. Comput. Mol. Sci.* **2014**, *4*, 49−61.
(21) Jin, H.; Goyal, P.; Das, A. K.; Gaus, M.; Meuwly, M.; Cui, Q. Copper Oxidation/Reduction in Water and Protein: Studies with DFTB3/MM and VALBOND Molecular Dynamics Simulations. *J. Phys. Chem. B* **2016**, *120*, 1894−1910.
(22) Lu, X.; Ovchinnikov, V.; Demapan, D.; Roston, D.; Cui, Q. Regulation and Plasticity of Catalysis in Enzymes: Insights from Analysis of Mechanochemical Coupling in Myosin. *Biochemistry* **2017**, *56*, 1482−1497.
(23) Markov, S.; Aradi, B.; Yam, C. Y.; Xie, H.; Frauenheim, T.; Chen, G. Atomic level modeling of extremely thin silicon-on-insulator MOSFETs including the silicon dioxide: Electronic structure. *IEEE Trans. Electron Devices* **2015**, *62*, 696−704.
(24) Kullgren, J.; Wolf, M. J.; Hermansson, K.; Köhler, C.; Aradi, B.; Frauenheim, T.; Broqvist, P. Self-Consistent-Charge Density-Functional Tight-Binding (SCC-DFTB) Parameters for Ceria in 0D to 3D. *J. Phys. Chem. C* **2017**, *121*, 4593−4607.
(25) Ohta, Y.; Okamoto, Y.; Irle, S.; Morokuma, K. Rapid growth of a single-walled carbon nanotube on an iron cluster: Density-functional tight-binding molecular dynamics simulations. *ACS Nano* **2008**, *2*, 1437−1444.
(26) Borlido, P.; Steigemann, C.; Lathiotakis, N. N.; Marques, M. A. L.; Botti, S. Structural prediction of two-dimensional materials under strain. *2D Mater.* **2017**, *4*, 045009.
(27) Sorkin, V.; Zhang, Y. Mechanical properties of phosphorene nanotubes: a density functional tight-binding study. *Nanotechnology* **2016**, *27*, 395701.
(28) Kohn, W.; Sham, L. J. Self-consistent equations including exchange and correlation effects. *Phys. Rev.* **1965**, *140*, A1133.
(29) Wahiduzzaman, M.; Oliveira, A. F.; Philipsen, P.; Zhechkov, L.; Van Lenthe, E.; Witek, H. A.; Heine, T. DFTB parameters for the periodic table: Part 1, electronic structure. *J. Chem. Theory Comput.* **2013**, *9*, 4006−4017.
(30) Knaup, J. M.; Hourahine, B.; Frauenheim, T. Initial Steps toward Automating the Fitting of DFTB $E_{rep}(r)$. *J. Phys. Chem. A* **2007**, *111*, 5637−5641.
(31) Gaus, M.; Chou, C.-P.; Witek, H.; Elstner, M. Automatized parametrization of SCC-DFTB repulsive potentials: Application to hydrocarbons. *J. Phys. Chem. A* **2009**, *113*, 11866−11881.
(32) Bodrog, Z.; Aradi, B.; Frauenheim, T. Automated repulsive parametrization for the DFTB method. *J. Chem. Theory Comput.* **2011**, *7*, 2654−2664.
(33) Lourenço, M. P.; da Silva, M. C.; Oliveira, A. F.; Quintão, M. C.; Duarte, H. A. FASP: a framework for automation of Slater-Koster file parameterization. *Theor. Chem. Acc.* **2016**, *135*, 250.
(34) Chou, C. P.; Nishimura, Y.; Fan, C. C.; Mazur, G.; Irle, S.; Witek, H. A. Automatized Parameterization of DFTB Using Particle Swarm Optimization. *J. Chem. Theory Comput.* **2016**, *12*, 53−64.
(35) Porezag, D.; Frauenheim, T.; Köhler, T.; Seifert, G.; Kaschner, R. Construction of tight-binding-like potentials on the basis of density-functional theory: Application to carbon. *Phys. Rev. B: Condens. Matter Mater. Phys.* **1995**, *51*, 12947−12957.
(36) Seifert, G.; Porezag, D.; Frauenheim, T. Calculations of molecules, clusters, and solids with a simplified LCAO-DFT-LDA scheme. *Int. J. Quantum Chem.* **1996**, *58*, 185−192.
(37) Seifert, G. Tight-binding density functional theory: An approximate Kohn-Sham DFT scheme. *J. Phys. Chem. A* **2007**, *111*, 5609−5613.
(38) Roothaan, C. C. J.; Sachs, L. M.; Weiss, A. W. Analytical self-consistent field functions for the atomic configurations 1s2, 1s22s, and 1s22s2. *Rev. Mod. Phys.* **1960**, *32*, 186−194.
(39) Woods, R. D.; Saxon, D. S. Diffuse surface optical model for nucleon-nuclei scattering. *Phys. Rev.* **1954**, *95*, 577−578.
(40) Witek, H. A.; Köhler, C.; Frauenheim, T.; Morokuma, K.; Elstner, M. Relativistic parametrization of the self-consistent-charge density-functional tight-binding method. 1. Atomic wave functions and energies. *J. Phys. Chem. A* **2007**, *111*, 5712−5719.
(41) Koskinen, P.; Mäkinen, V. Density-functional tight-binding for beginners. *Comput. Mater. Sci.* **2009**, *47*, 237−253.
(42) Perdew, J. P.; Burke, K.; Ernzerhof, M. Generalized gradient approximation made simple. *Phys. Rev. Lett.* **1996**, *77*, 3865.
(43) Kresse, G.; Furthmüller, J. Efficient iterative schemes for ab initio total-energy calculations using a plane-wave basis set. *Phys. Rev. B: Condens. Matter Mater. Phys.* **1996**, *54*, 11169.

DOI: 10.1021/acs.jctc.7b01269
J. Chem. Theory Comput. 2018, 14, 2947−2954

(44) Oganov, A. R. *Modern methods of crystal structure prediction*; John Wiley & Sons: 2011; DOI: 10.1002/9783527632831.
(45) Goedecker, S. Minima hopping: An efficient search method for the global minimum of the potential energy surface of complex molecular systems. *J. Chem. Phys.* **2004**, *120*, 9911−9917.
(46) Amsler, M.; Goedecker, S. Crystal structure prediction using the minima hopping method. *J. Chem. Phys.* **2010**, *133*, 224104.
(47) Shi, J.; Cerqueira, T. F.; Cui, W.; Nogueira, F.; Botti, S.; Marques, M. A. L. High-throughput search of ternary chalcogenides for p-type transparent electrodes. *Sci. Rep.* **2017**, *7*, 43179.
(48) Artrith, N.; Urban, A. An implementation of artificial neural-network potentials for atomistic materials simulations: Performance for TiO2. *Comput. Mater. Sci.* **2016**, *114*, 135−150.
(49) Kim, I. Y.; de Weck, O. L. Adaptive weighted-sum method for bi-objective optimization: Pareto front generation. *Struct. Multidiscip. Optim.* **2005**, *29*, 149−158.
(50) Kim, I. Y.; De Weck, O. Adaptive weighted sum method for multiobjective optimization: a new method for Pareto front generation. *Struct. Multidiscip. Optim.* **2006**, *31*, 105−116.
(51) Fortin, F.-A.; Rainville, F.-M. D.; Gardner, M.-A.; Parizeau, M.; Gagné, C. DEAP: Evolutionary algorithms made easy. *J. Mach. Learn. Res.* **2012**, *13*, 2171−2175.
(52) Knysh, P.; Korkolis, Y. Blackbox: A procedure for parallel optimization of expensive black-box functions. *arXiv:1605.00998* 2016.
(53) Shoemaker, C.; Pang, M.; Akhtar, T.; Bindel, D. Applications of New Surrogate Global Optimization Algorithms including Efficient Synchronous and Asynchronous Parallelism for Calibration of Expensive Nonlinear Geophysical Simulation Models, AGU Fall Meeting Abstracts, 2016.
(54) Hooke, R.; Jeeves, T. A. Direct Search"Solution of Numerical and Statistical Problems. *J. Assoc. Comput. Mach.* **1961**, *8*, 212−229.
(55) Adams, B. M.; Bauman, L. E.; Bohnhoff, W. J.; Dalbey, K. R.; Ebeida, M. S.; Eddy, J. P.; Eldred, M. S.; Hough, P. D.; Hu, K. T.; Jakeman, J. D.; Stephens, J. A.; Swiler, L. P.; Vigil, D. M.; Wildey, T. M. DAKOTA, a multilevel parallel object-oriented framework for design optimization, parameter estimation, uncertainty quantification, and sensitivity analysis: version 6.6 user's manual; *Tech. Rep. SAND2014-4633*; Sandia National Laboratories: 2017.
(56) Torczon, V. On the convergence of pattern search algorithms. *SIAM J. Optim.* **1997**, *7*, 1−25.
(57) Dolan, E. D.; Lewis, R. M.; Torczon, V. On the local convergence of pattern search. *SIAM J. Optim.* **2003**, *14*, 567−583.
(58) Aradi, B.; Hourahine, B.; Frauenheim, T. DFTB+, a sparse matrix-based implementation of the DFTB method. *J. Phys. Chem. A* **2007**, *111*, 5678−5684.
(59) Larsen, A. H.; Mortensen, J. J.; Blomqvist, J.; Castelli, I. E.; Christensen, R.; Dułak, M.; Friis, J.; Groves, M. N.; Hammer, B.; Hargus, C.; Hermes, E. D.; Jennings, P. C.; Jensen, P. B.; Kermode, J.; Kitchin, J. R.; Kolsbjerg, E. L.; Kubal, J.; Kaasbjerg, K.; Lysgaard, S.; Maronsson, J. B.; Maxson, T.; Olsen, T.; Pastewka, L.; Peterson, A.; Rostgaard, C.; Schiøtz, J.; Schütt, O.; Strange, M.; Thygesen, K. S.; Vegge, T.; Vilhelmsen, L.; Walter, M.; Zeng, Z.; Jacobsen, K. W. The atomic simulation environment-a Python library for working with atoms. *J. Phys.: Condens. Matter* **2017**, *29*, 273002.
(60) Tran, F.; Stelzl, J.; Blaha, P. Rungs 1 to 4 of DFT Jacob's ladder: Extensive test on the lattice constant, bulk modulus, and cohesive energy of solids. *J. Chem. Phys.* **2016**, *144*, 204120.
(61) Sarmiento-Pérez, R.; Botti, S.; Marques, M. A. L. Optimized exchange and correlation semilocal functional for the calculation of energies of formation. *J. Chem. Theory Comput.* **2015**, *11*, 3844−3850.
(62) Stevanović, V.; Lany, S.; Zhang, X.; Zunger, A. Correcting density functional theory for accurate predictions of compound enthalpies of formation: Fitted elemental-phase reference energies. *Phys. Rev. B: Condens. Matter Mater. Phys.* **2012**, *85*, 115104.
(63) Sieck, A. Structure and Physical Properties of Si Clusters and Vacancy Clusters in Bulk Si. Ph.D. thesis, Paderborn Univ., 2000.
(64) Köhler, C.; Hajnal, Z.; Deák, P.; Frauenheim, T.; Suhai, S. Theoretical investigation of carbon defects and diffusion in α-quartz. *Phys. Rev. B: Condens. Matter Mater. Phys.* **2001**, *64*, 085333.
(65) Frenzel, J.; Oliveira, A.; Jardillier, N.; Heine, T.; Seifert, G. Semi-relativistic, self-consistent charge Slater- Koster tables for density-functional based tight-binding (DFTB) for materials science simulations. *Zeolites* **2004**, *2*, 7.
(66) Gaus, M.; Goez, A.; Elstner, M. Parametrization and benchmark of DFTB3 for organic molecules. *J. Chem. Theory Comput.* **2013**, *9*, 338−354.
(67) Trani, F.; Barone, V. Silicon Nanocrystal Functionalization: Analytic Fitting of DFTB Parameters. *J. Chem. Theory Comput.* **2011**, *7*, 713−719.
(68) Stewart, J. J. Optimization of parameters for semiempirical methods V: modification of NDDO approximations and application to 70 elements. *J. Mol. Model.* **2007**, *13*, 1173−1213.
(69) Murnaghan, F. The compressibility of media under extreme pressures. *Proc. Natl. Acad. Sci. U. S. A.* **1944**, *30*, 244−247.
(70) Togo, A.; Tanaka, I. First principles phonon calculations in materials science. *Scr. Mater.* **2015**, *108*, 1−5.

DOI: 10.1021/acs.jctc.7b01269
J. Chem. Theory Comput. 2018, 14, 2947−2954